Calcium-activated chloride currents in olfactory sensory neurons from mice lacking bestrophin-2

Simone Pifferi[1], Michele Dibattista[1], Claudia Sagheddu[1], Anna Boccaccio[1], Ahmed Al Qteishat[1], Filippo Ghirardi[2], Roberto Tirindelli[2] and Anna Menini[1]

[1]*International School for Advanced Studies, Scuola Internazionale Superiore di Studi Avanzati, SISSA, and Italian Institute of Technology, SISSA Unit, Trieste, Italy*
[2]*Section of Physiology, Department of Neuroscience, University of Parma, Parma, Italy*

Olfactory sensory neurons use a chloride-based signal amplification mechanism to detect odorants. The binding of odorants to receptors in the cilia of olfactory sensory neurons activates a transduction cascade that involves the opening of cyclic nucleotide-gated channels and the entry of Ca^{2+} into the cilia. Ca^{2+} activates a Cl^- current that produces an efflux of Cl^- ions and amplifies the depolarization. The molecular identity of Ca^{2+}-activated Cl^- channels is still elusive, although some bestrophins have been shown to function as Ca^{2+}-activated Cl^- channels when expressed in heterologous systems. In the olfactory epithelium, bestrophin-2 (Best2) has been indicated as a candidate for being a molecular component of the olfactory Ca^{2+}-activated Cl^- channel. In this study, we have analysed mice lacking Best2. We compared the electrophysiological responses of the olfactory epithelium to odorant stimulation, as well as the properties of Ca^{2+}-activated Cl^- currents in wild-type (WT) and knockout (KO) mice for Best2. Our results confirm that Best2 is expressed in the cilia of olfactory sensory neurons, while odorant responses and Ca^{2+}-activated Cl^- currents were not significantly different between WT and KO mice. Thus, Best2 does not appear to be the main molecular component of the olfactory channel. Further studies are required to determine the function of Best2 in the cilia of olfactory sensory neurons.

Abbreviations Best2, bestrophin-2; CNG, cyclic nucleotide-gated; KO, knockout; WT, wild-type.

In vertebrates, the process of olfactory transduction occurs in sensory neurons, located in the olfactory epithelium in the nasal cavity. Each olfactory sensory neuron bears several cilia departing from the knob-like swelling of the apical part of the dendrite. The cilia are the site of olfactory transduction: odorant molecules bind to specific receptors expressed in the ciliary plasma membrane activating a G protein-coupled transduction cascade. The activation of adenylyl cyclase by the G protein produces an increase in the ciliary concentration of cAMP, which opens cyclic nucleotide-gated (CNG) channels, which produces a primary inward current carried by Na^+ and Ca^{2+} ions (reviewed by Schild & Restrepo, 1998; Menini, 1999; Firestein, 2001; Matthews & Reisert, 2003; Menini *et al.* 2004; Pifferi *et al.* 2006*a*; Kleene, 2008). The increase in

Ca^{2+} concentration triggers the gating of Ca^{2+}-activated Cl^- channels that gives rise to a secondary Cl^- current. Since olfactory sensory neurons maintain an elevated intracellular Cl^- concentration, which is in the same range of the Cl^- concentration present in the mucus at the external side of the cilia (Reuter *et al.* 1998; Kaneko *et al.* 2001, 2004), the opening of Ca^{2+}-activated Cl^- channels in the ciliary membrane causes an efflux of Cl^- ions from the cilia, which amplifies the primary inward current (Kleene & Gesteland, 1991; Kleene, 1993; Kurahashi & Yau, 1993; Lowe & Gold, 1993; Kleene, 1997; Boccaccio & Menini, 2007; reviewed by Frings *et al.* 2000; Kleene, 2008; Frings, 2009).

While most of the components of the olfactory transduction cascade have been identified at the molecular level, the molecular identity of Ca^{2+}-activated Cl^- channels is still elusive. In recent years, several proteins have been proposed as possible candidates for Ca^{2+}-activated Cl^-

---

S. Pifferi and M. Dibattista contributed equally to this study.

channels, including the families of bestrophins, tweety, CLCA calcium activated chloride channels (reviewed by Hartzell *et al.* 2005, 2009) and, very recently, the anoctamin/transmembrane 16 (TMEM16) protein family (Caputo *et al.* 2008; Schroeder *et al.* 2008; Yang *et al.* 2008; Pifferi *et al.* 2009; Stephan *et al.* 2009).

Proteins of the bestrophin family have been shown to form Cl^- channels when expressed in heterologous systems (Sun *et al.* 2002; Tsunenari *et al.* 2003) and have been proposed to be *bona fide* Ca^{2+}-activated Cl^- channels (Qu *et al.* 2003, 2004; Pusch, 2004), although other reports suggested that they function as regulators of ion transport rather than as ion channels (Rosenthal *et al.* 2006; Yu *et al.* 2008; reviewed by Kunzelmann *et al.* 2007; Hartzell *et al.* 2008; Marmorstein *et al.* 2009).

We have previously shown that bestrophin-2 (Best2) is expressed in the cilia of mouse olfactory sensory neurons, where it colocalizes with CNGA2, the principal subunit of the olfactory CNG channel that is responsible for the primary transduction current (Pifferi *et al.* 2006*b*). Moreover, we have shown that the functional properties of the current induced by heterologous expression of mouse Best2 and those of the native Ca^{2+}-activated Cl^- current from dendritic knob/cilia of mouse olfactory sensory neurons present many similarities, including the same anion permeability sequence, small estimated single-channel conductances, and the same side-specific blockage by some Cl^- channel blockers, although also differences do exist and include a Ca^{2+} sensitivity discrepancy of one order of magnitude (Pifferi *et al.* 2006*b*). However, based on the overall findings, Best2 was indicated to be candidate molecular component of Ca^{2+}-activated Cl^- channels involved in olfactory transduction (Pifferi *et al.* 2006*b*). In the last year knockout mice for Best2 became commercially available opening the possibility of further investigation of the physiological role of Best2. We have therefore analysed the responses of the olfactory epithelium to odorant stimulation and investigated the properties of Ca^{2+}-activated Cl^- currents in wild-type (WT) and knockout (KO) mice lacking Best2. Our results confirm that Best2 is expressed in the cilia of olfactory sensory neurons, but we found that Ca^{2+}-activated Cl^- currents were not significantly different between WT and KO mice, indicating that Best2 is not the main molecular component of the olfactory channel. Further studies are required to determine the physiological role of Best2 in the cilia of olfactory sensory neurons.

Methods

Ethical approval

All animals were handled in accordance with the Italian Guidelines for the Use of Laboratory Animals (Decreto Legislativo 27/01/1992, no. 116) and European Union guidelines on animal research (No. 86/609/EEC). For experiments mice were anaesthetized by CO_2 inhalation and then decapitated.

Animals

Experiments were performed on knockout (KO) mice for *Best2* and wild-type (WT) littermates between 2 and 6 months of age. *Best2* homozygous mutant and WT mice were obtained by breeding heterozygous mutant mice obtained from Deltagen (San Mateo, CA, USA). The generation of these mice has been previously described in detail (Bakall *et al.* 2008).

Cookie test

Mice were left overnight without food with water *ad libitum*. The next day, mice were moved into an opaque cage, while a food pellet (Altromin-R, A. Rieper S.p.A., Vandoies, Bolzano, Italy) was buried in their litter's sawdust, about 2 cm underneath. Then, mice were brought back in their cages and released at the centre of the litter. The time was measured from the moment they were freed to the moment they found the pellet. Results were analysed using the analysis software SPSS 13.0 (SPSS Inc., Chicago, IL, USA) and StatView (SAS Institute Inc., Cary, NC, USA).

RNA isolation and RT-PCR

Total RNA was extracted from the olfactory epithelium of WT and KO mice using standard Clontech procedures (BD Biosciences, Hertfordshire, UK). RNA quality was measured using a NanoDrop1000 Spectrophotometer (ND-1000). Gene expression was examined by RT-PCR from total RNA using primers designed against *Best2*, *CNGA2* and the housekeeping gene *S16*. PCR conditions were as follows: an initial denaturation step of 10 min at 95°C, followed by 35 cycles of 1 min at 94°C, 1 min at 58°C and 1 min at 72°C, and a final extension step of 10 min at 72°C. The products were visualized following agarose gel electrophoresis (1.5%) and DNA was stained with ethidium bromide (10 mg ml^{-1}). Samples without cDNA were used as negative controls. The sequences of the primers used were the following:

Best2 (forward: 5′-AGT CCC AGG AAA CAT AAC AGC TCT C-3′ and reverse: 5′-CTC CCA GCA TCT TCC CTT GGC TCA C-3′);
CNGA2 (forward: 5′-AGG GAA AGG GCA CCA AAA AGA AA-3′ and reverse: 5′-CCA GCA CCA GCC ATA CCA CAA A-3′);

S16 (forward: 5′-GGC AGA CCG AGA TGA ATC CTC A-3′ and reverse: 5′-CAG GTC CAG GGG TCT TGG TCC-3′).

Western blot

Proteins were extracted from olfactory epithelium tissues by RIPA buffer (Millipore, Milan, Italy) and the protein concentration of each sample was determined using the Bio-Rad assay. For Western blotting, 10 μg of protein was separated by gel electrophoresis (SDS-PAG; 12% w/v) and the proteins were electro-blotted onto nitrocellulose filters (Whatman, Germany). Filters were blocked in 1% w/v bovine serum albumin (BSA) in Tris-buffered saline Tween 20 (TBS Tween) and incubated overnight at 4°C with the following primary antibodies: rabbit polyclonal anti-Best2 (1:500; Pifferi *et al.* 2006*b*); mouse mono-clonal anti-CNGA2 (a gift from F. Müller and U. B. Kaupp, Forschungszentrum Julich, Julich, Germany; Meyer *et al.* 2000), and anti-β-actin (1:1000; Sigma, Milan, Italy). Membranes were washed in TBS-Tween before staining with antibodies to the appropriate peroxidase-conjugated secondary antibody, diluted 1:1000 in 1% w/v BSA in TBS Tween for 1 h. Blots were developed with the ECL detection system (Amersham, UK).

Immunohistochemistry

The nasal regions were fixed in 4% paraformaldehyde for 4 h at 4°C, decalcified by overnight incubation in 0.5 M EDTA, and then equilibrated in 30% (w/v) sucrose overnight at 4°C for cryoprotection. Coronal sections 16 μm thick were cut on a cryostat and stored at −20°C. Tissue sections were incubated with 0.5% sodium dodecyl sulfate (v/v) in phospate buffered saline (PBS) for 15 min for antigen retrieval, then incubated in blocking solution (2% normal goat serum, 0.2% Triton X-100 in PBS) for 90 min, and incubated overnight at 4°C in primary antibodies diluted in blocking solution. After rinsing in 0.1% (v/v) Tween 20 in PBS, sections were incubated with fluorophore-conjugated secondary antibodies in 0.1% Tween 20 in PBS for 2 h at room temperature and washed. 4′-6-Diamidino-2-phenylindole (DAPI) (0.1 μg ml^{-1}) was used to stain nuclei: tissue sections were incubated for 30 min then washed and mounted with Vectashield (Vector Laboratories, Burlingame, CA, USA).

Primary antibodies were rabbit anti-Best2 (Pifferi *et al.* 2006*b*) and mouse monoclonal anti-CNGA2 (Meyer *et al.* 2000) used at 1:50. Secondary antibodies were Alexa 488-conjugated goat anti-rabbit and Alexa 594-conjugated goat anti-mouse diluted to 1:200 (Molecular Probes-Invitrogen, Eugene, OR, USA).

Images were visualized by Leica TCS SP2 confocal microscope, acquired using Leica software at 1024 × 1024 pixels resolution and analysed with ImageJ software.

Electro-olfactograms

Electro-olfactogram (EOG) recordings were performed as previously described (Franceschini *et al.* 2009). The mouse head was cut sagitally to expose the medial surface of the olfactory turbinates and EOG recordings were measured at the surface of the olfactory epithelium in response to odorant stimuli in the vapour phase. Each odorant, amylacetate, cineole and acetophenone (Sigma, Milan, Italy), was prepared as 2.5 M stock in DMSO and then diluted with water to the final concentrations used in the experiments. Responses to DMSO alone were less than 0.05 mV. Vapour-phase odorant stimuli were generated by placing 0.9 ml of an odorant solution in a 10 ml glass test-tube capped with a rubber stopper. For stimulation, a 100 ms pulse of the odorant vapour at 8 psi was injected into a continuous stream of humidified air.

Electrophysiological recordings from dissociated olfactory sensory neurons

Olfactory sensory neurons were dissociated enzymatically from the olfactory epithelium of 1- to 2-month-old mice, with a papain–cysteine treatment as previously described (Lagostena & Menini, 2003; Boccaccio *et al.* 2006). Cells were plated on Petri dishes for excised patch recordings, or on glass coverslips coated with poly-L-lysine and concanavalin A (Type V, Sigma, Milan, Italy) for whole-cell recordings with photolysis of caged compounds (Boccaccio *et al.* 2006; Boccaccio & Menini, 2007).

Currents in the whole-cell or in the inside-out voltage-clamp modes were recorded with an Axopatch 1D or an Axopatch 200B amplifier controlled by Clampex 8 or 9 via a Digidata 1322A or 1332A (Axon Instruments, Union City, CA, USA). Patch pipettes were made using borosilicate capillaries (WPI, Sarasota, FL, USA) and pulled with a Narishige PP83 puller (Narishige, Tokyo, Japan). Patch pipettes filled with standard intracellular solutions had resistances of 2–7 MΩ for whole-cell and 7–10 MΩ for excised patch recordings. Currents were low-pass filtered at 1 kHz and acquired at 2 kHz for whole-cell experiments, or filtered at 4 kHz and sampled at 10 kHz for excised patch recordings. All experiments were carried out at room temperature (20–22°C).

For flash photolysis of the caged compounds, we used a xenon flash-lamp system, JML-C2 (Rapp OptoElectronic, Hamburg, Germany), coupled with the epifluorescence port of the microscope with a quartz light guide (Boccaccio *et al.* 2006). The spot of light had a diameter of about 15 μm and was focused on the ciliary region. The interval

between experiments was about 2 min to allow the cell to recover from adaptation.

Rapid solution exchange in inside-out patches was obtained with the perfusion Fast-Step SF-77B (Warner Instrument Corp., Hamden, CT, USA). For current–voltage relations of Ca^{2+}-activated currents, inside-out patches were pre-exposed to the test Ca^{2+} concentration for 500 ms at -100 mV to allow the current to partially inactivate, and then a double voltage ramp from -100 to $+100$ mV and back to -100 mV was applied at 1 mV ms^{-1}. The two current–voltage relations were averaged and leak currents measured with the same ramp protocol in Ca^{2+}-free solutions were subtracted. The same type of voltage protocol was used to measure current–voltage relations of cAMP-activated currents.

Ionic solutions

For whole-cell recordings, the extracellular mammalian Ringer solution contained (in mM): 140 NaCl, 5 KCl, 1 $CaCl_2$, 1 $MgCl_2$, 10 Hepes, 10 glucose and 1 sodium pyruvate (pH 7.4). The composition of the low Ca^{2+} extracellular solution was similar, except that it contained 10 mM EGTA and no added Ca^{2+}. The whole-cell pipette solution for the photorelease of caged 8-Br-cAMP contained (in mM): 145 KCl, 4 $MgCl_2$, 0.5 EGTA, 10 Hepes, 1 MgATP, 0.1 GTP, 0.05 caged 8-Br-cAMP, (pH 7.4). The caged BCMCM-8-Br-cAMP (Boccaccio *et al.* 2006) was dissolved in DMSO at 10 or 50 mM and stored at -20°C for up to 3 months. The final concentration of 50 μM was obtained by diluting an aliquot of the stock solution into the pipette solution, kept refrigerated in the dark during the experimental session, and stored for a few days at -20°C. The standard pipette solution for the photorelease of caged Ca^{2+} contained (in mM): 3 DMNP-EDTA, 1.5 $CaCl_2$, 140 KCl, and 10 Hepes (pH 7.4). The low Cl^- intracellular solutions for the photorelease of caged Ca^{2+} contained (in mM): 3 DMNP-EDTA, 1.5 $CaCl_2$, 12 KCl, 133 potassium gluconate, and 10 Hepes (pH 7.4). Liquid junction potentials were corrected off-line. DMNP-EDTA was purchased from Molecular Probes–Invitrogen, and $CaCl_2$ was adjusted with a 0.1 M standard solution from Fluka (Deisenhofen, Germany). The caged compounds were allowed to diffuse from the patch pipette into the cytoplasm of an olfactory sensory neuron for about 2 min after establishment of the whole-cell configuration.

For inside-out recordings, the standard solution in the patch pipette contained (in mM): 140 NaCl, 10 HEDTA and 10 Hepes, pH 7.2. In experiments for Ca^{2+} dose–response relations, NaCl was replaced with LiCl to inhibit the Na^+/Ca^{2+} exchanger. The bathing solution at the intracellular side of the patch contained (in mM): 140 NaCl or LiCl, 10 HEDTA and 10 Hepes, pH 7.2, and no added Ca^{2+} for the nominally 0 Ca^{2+} solution, or

various added Ca^{2+} concentrations, as calculated with the program WinMAXC (C. Patton), to obtain free Ca^{2+} in the range between 1.5 and 100 μM (Patton *et al.* 2004). The free Ca^{2+} concentrations were experimentally determined by Fura-4F (Molecular Probes–Invitrogen) measurements by using an LS-50B luminescence spectrophotometer (PerkinElmer, Wellesley, MA, USA). To activate CNG channels a solution containing 100 μM cAMP directly dissolved into the 0 Ca^{2+} bathing solution was used.

Chemicals, unless otherwise stated, were purchased from Sigma (Milan, Italy).

Data analysis

Data are reported as means $\pm$ standard deviation, with the number of experiments (n) from different mice, cells or membrane patches, as appropriate. The statistical significance of data was evaluated by Student's t-test and P values < 0.05 were considered significant. Data analysis and figures were made with Igor software (Wavemetrics, Lake Oswego, OR, USA).

Results

Expression of *Best2* in the olfactory epithelium

To examine the expression of *Best2*, we performed RT-PCR on total RNA from the olfactory epithelium of WT and KO mice. Specific primers for *Best2*, for the main subunit of the CNG channel *Cnga2*, and for the housekeeping gene *S16* showed that, in WT mice, PCR products of the predicted size were amplified (Best2, 205 bp; CNGA2, 200 bp; S16, 102 bp) (Fig. 1*A*). In KO mice, the 205 bp reaction product, corresponding to *Best2*, was absent, while control genes were normally expressed (Fig. 1*A*). This result confirms the absence of expression of *Best2* in the olfactory epithelium of KO mice.

Best2 immunoreactivity in the olfactory epithelium

To verify the lack of expression of the Best2 protein in the olfactory epithelium of KO mice, we performed both Western blotting and immunohistochemistry (Fig. 1*B* and *C*), using the antibody against Best2 that we have previously generated and characterized (Pifferi *et al.* 2006*b*).

By Western blotting, we identified a 57 kDa band in a membrane fraction of the olfactory epithelium of WT mice, corresponding to the expected molecular weight for the Best2 protein, in agreement with our previous study (Pifferi *et al.* 2006*b*). The 57 kDa band was undetectable in KO animals, while both the 75 and 42 kDa bands, corresponding respectively to CNGA2 and β-actin, were expressed in both mouse lines (Fig. 1*B*).

By immunohistochemistry, we confirmed our previous results showing that Best2 is expressed in the olfactory epithelium of WT mice (Pifferi *et al.* 2006*b*). We found staining at the surface of the olfactory epithelium, at the level of the ciliary layer, where Best2 colocalized with CNGA2 (Fig. 1*C*, top panels). In the olfactory epithelium of KO mice, Best2 immunoreactivity was absent, while CNGA2 was normally expressed at the level of the ciliary layer (Fig. 1*C*, bottom panels). These results demonstrate the loss of the Best2 protein in the olfactory epithelium of KO mice and confirm the specificity of our antibody against this protein.

Behavioural olfactory response

To determine whether deletion of *Best2* caused a behavioural olfactory deficit, mice were examined for olfactory function in a cookie-finding test. In this test, we compared the food-finding ability of WT and KO mice by measuring the latency to locate buried food. Mice were food-deprived with free access to water overnight and then were put in a cage where a food pellet was buried under the litter. None of the mice searched randomly in the litter; conversely, they dug only in the place where the pellet was hidden. The average time necessary to locate the cookie

was 55 ± 32 s ($n = 22$) for WT mice, similar to 62 ± 34 s ($n = 22$) for KO animals. These results show that KO mice do not exhibit any gross olfactory deficit, in agreement with previous results (Bakall *et al.* 2008).

Odorant-induced responses in WT and KO mice

To investigate whether disruption of the *Best2* gene modifies the odorant sensitivity of olfactory sensory neurons, we measured odorant-induced changes in voltage across the olfactory epithelium of WT and KO mice. Indeed, the electrical activity of a population of olfactory sensory neurons in response to odorants can be recorded at the surface of the olfactory epithelium as a negative electrical field potential, the electro-olfactogram (EOG) (Ottoson, 1955; Scott & Scott-Johnson, 2002). EOG responses induced by delivering the vapour phase of a 2.5 M amyl acetate solution for 100 ms to the olfactory epithelium were recorded at 13 different locations as indicated in Fig. 2*A*. Although the amplitudes of EOG responses varied according to the different subregions of the olfactory epithelium, amplitudes at each specific location were not significantly different between WT and KO mice (Fig. 2*B*). Similar results were obtained with two
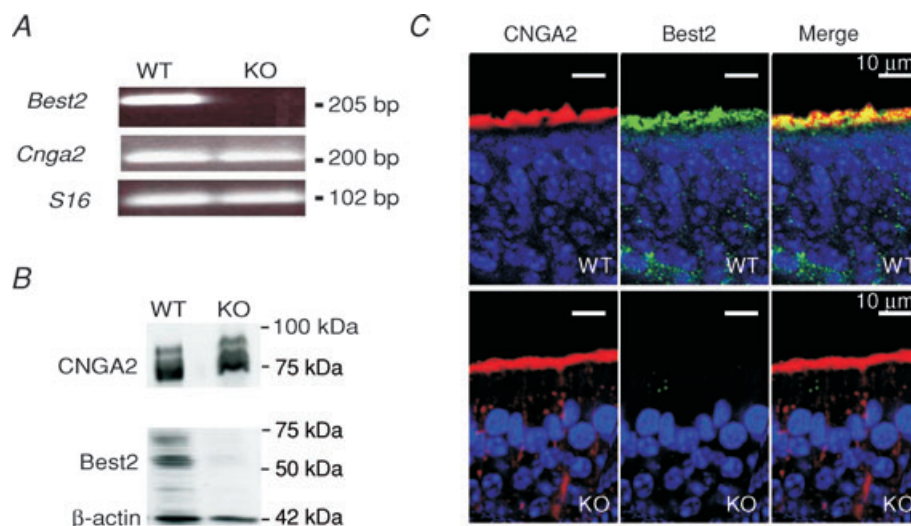
Figure 1. Comparison of Best2 mRNA expression and Best2 immunoreactivity in the mouse olfactory epithelium of WT and KO mice
A, reverse transcription–polymerase chain reaction (RT-PCR) derived cDNA products amplified from RNA of the olfactory epithelium in WT and KO mice using specific primers for *Best2*, *CNGA2* and *S16*, as indicated in the figure. The predicted size of the products for *Best2*, *CNGA2* and *S16* was respectively 205, 200 and 102 base pairs (bp). *B*, Western blot analysis of proteins of the olfactory epithelium in WT and KO mice probed with antibodies against Best2, CNGA2 and β-actin. Bands of the appropriate molecular mass were observed for each protein in WT mice, whereas only bands corresponding to CNGA2 and β-actin were detected in KO mice. The expected molecular mass for Best2, CNGA2 and β-actin was respectively 57, 75 and 42 kDa. *C*, immunostaining of sections of the olfactory epithelium. Confocal micrographs showing Best2 and CNGA2 expression in the ciliary layer of the olfactory epithelium of WT and KO mice. CNGA2 and Best2 co-expression was evident in WT mice, whereas no immunoreactivity to Best2 was detectable in KO mice. Each image on the right was obtained from the merge of the respective left and centre images. Cell nuclei were stained by DAPI.

other commonly used odorants: acetophenone and cineole (data not shown).

We determined the dose–response relation in response to amyl acetate by delivering the vapour phase of odorant solutions at various concentrations to the olfactory epithelium. Figure 2C shows representative recordings of EOG responses to amyl acetate in WT and KO mice. The odorant concentration producing 50% of the maximal EOG amplitude was about 10^{-3} M for both WT and KO mice (Fig. 2D).

We further analysed the kinetics of the EOG recordings. We measured the latency of the response as the interval between the beginning of the odorant application and the time at which the response reached 1% of its maximal value, the rise time as the time interval between 1% and the peak EOG response, and the termination as the time constant of the exponential fit of the recovery phase of the EOG response from the peak value to 10% of the peak. We did not find any significant difference for any of these parameters between WT and KO mice (Fig. 3).

Thus, no differences were observed between KO and WT mice in EOG recordings, indicating that the absence of Best2 does not significantly affect responses to odorants. However, we cannot exclude the possibility that EOG
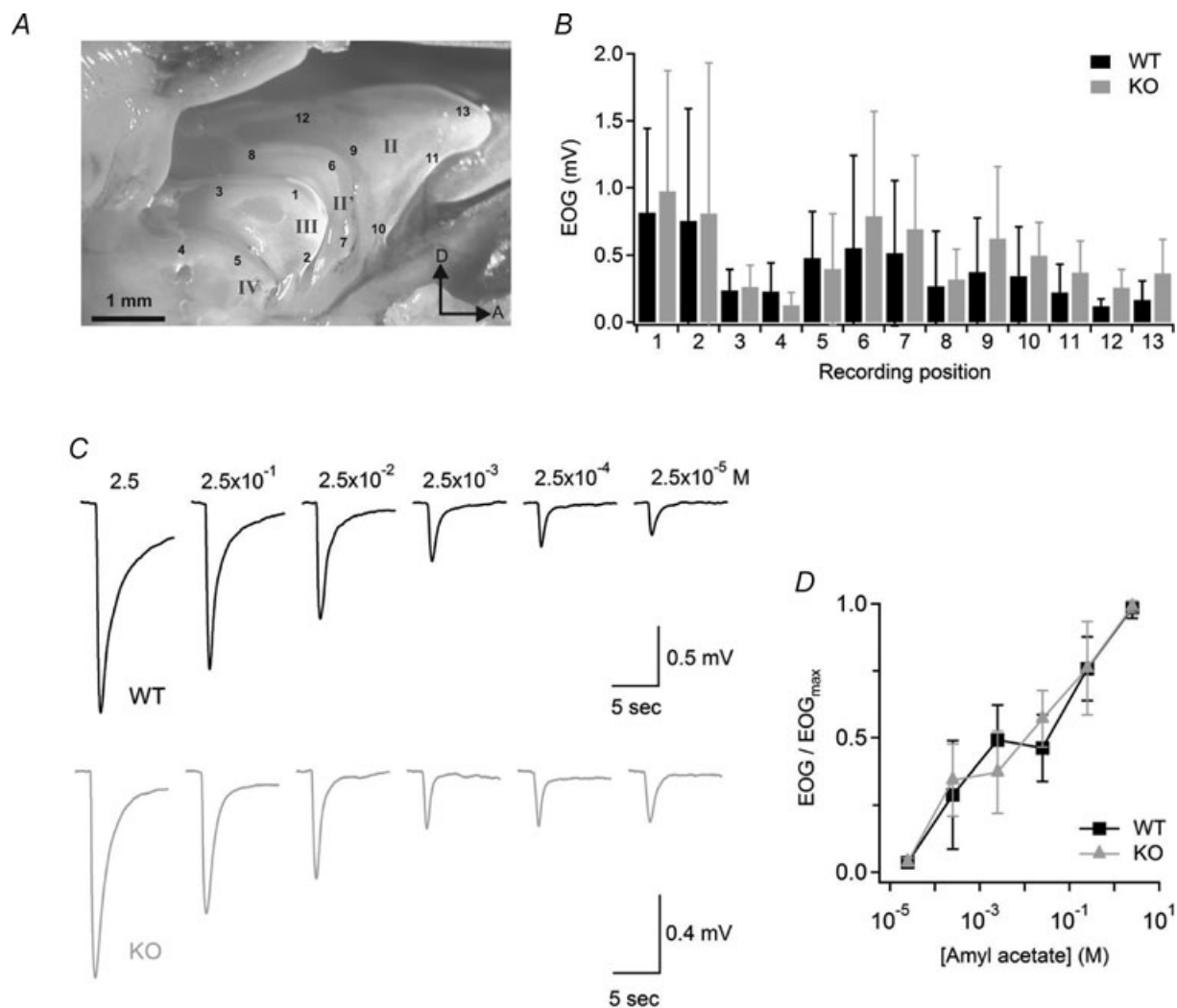
Figure 2. Odorant sensitivity in WT and KO mice
A, photomicrograph of the olfactory turbinate system. Roman numbers designate individual turbinates. Arabic numbers indicate the locations where EOG responses were recorded. D, dorsal; A, anterior. B, average EOG amplitudes in response to a 100 ms pulse of odorant vapour from a bottle containing 2.5 M amyl acetate liquid solution measured at the locations indicated in A (n = 7–14). C, representative EOG recordings from WT (black traces) or KO (grey traces) mice in response to 100 ms pulses of amyl acetate vapours. Numbers above traces are the concentrations of amyl acetate solutions in the bottle. EOG recordings were from location 1. D, EOG amplitudes were normalized to the value measured in response to the vapour of a 2.5 M amyl acetate solution, averaged, and plotted *versus* amyl acetate concentrations in solution for WT (n = 14; black symbols) or KO (n = 13, grey symbols) mice. Data points are linked with straight lines.

recordings are similar in WT and KO animals because some compensatory mechanism may modify the intraciliary ion concentrations in KO compared to WT mice. Indeed, although EOG measurements have the advantage of allowing long recordings while leaving the neurons in a relatively unperturbed situation, this technique does not allow the control of the intracellular ionic composition of neurons and of the membrane potential.

Currents in isolated olfactory sensory neurons

To achieve a control of both the intracellular and extracellular ionic compositions, as well as of voltage, we used isolated olfactory sensory neurons and the patch-clamp technique in the whole-cell voltage-clamp configuration. To investigate whether a Ca^{2+}-activated Cl^{-} current was present in individual olfactory sensory neurons from WT and KO mice, we measured the transduction current directly activating CNG channels in the cilia (Fig. 4). Indeed, the use of odorants to activate the transduction current in isolated olfactory sensory neurons would produce a very low probability of measuring odorant responses (Lagostena & Menini, 2003), due to the fact that each olfactory sensory neuron expresses only one of more than a thousand odorant receptors (for reviews, see Rodriguez, 2007; Malnic, 2007). To activate CNG channels in the cilia, we included caged 8-Br-cAMP in the intracellular solution filling the patch pipette and applied ultraviolet light flashes to the ciliary region to release the physiologically active 8-Br-cAMP. Upon flash photolysis, CNG channels are activated by 8-Br-cAMP allowing the flux of Ca^{2+} ions in the cilia and the subsequent opening of Ca^{2+}-activated Cl^{-} channels (Boccaccio *et al.* 2006; Boccaccio & Menini, 2007). We have previously shown that the rising phase of the response at -50 mV in Ringer solution containing 1 mM Ca^{2+} was multiphasic, composed of a primary phase of the response due to Na^{+} and Ca^{2+} influx through CNG channels and a secondary phase due to Cl^{-} efflux through Cl^{-} channels activated by the influx of Ca^{2+}. Moreover, the secondary phase of the response was absent in low extracellular Ca^{2+} or at $+50$ mV, when the influx of Ca^{2+} through CNG channels is strongly reduced and therefore the contribution of Ca^{2+}-activated Cl^{-} channels is expected to be negligible (Boccaccio & Menini, 2007).

To investigate the Ca^{2+} dependence of the rising phase of the response in WT and KO mice, we compared responses at -50 mV in extracellular low Ca^{2+} or in 1 mM Ca^{2+} in the same neuron (Fig. 4*A* and *B*). Both in WT and in KO mice the rising phase of the response in low Ca^{2+} was well
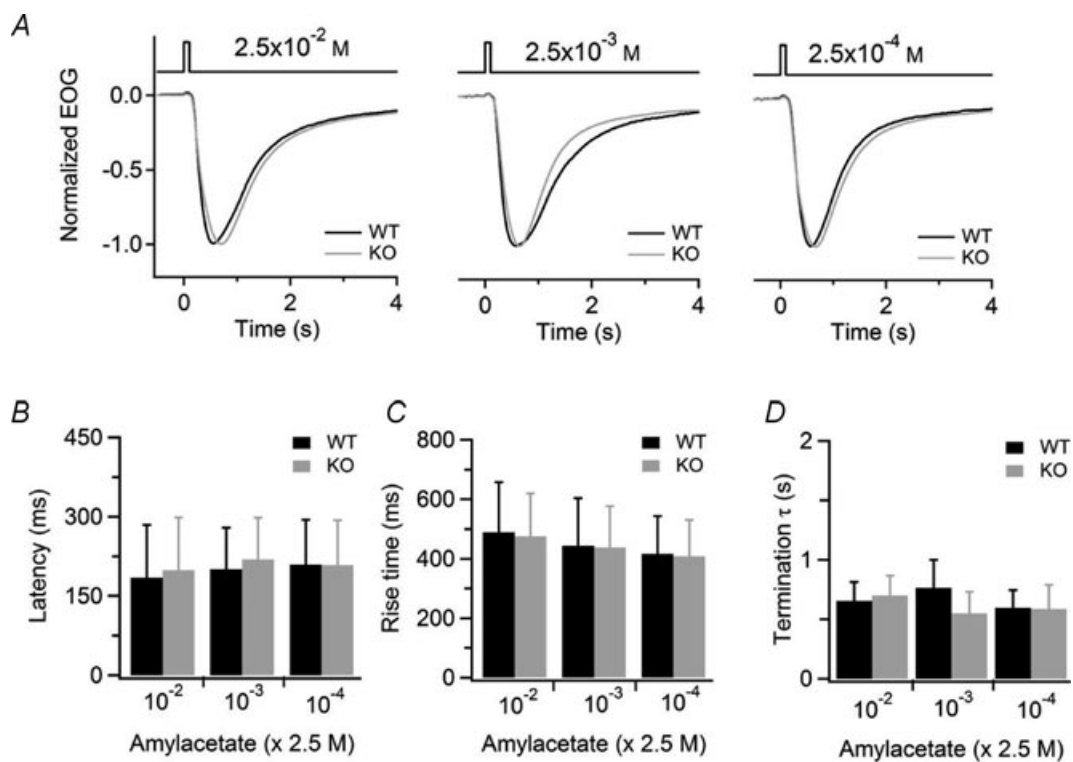

Figure 3. Kinetics analysis of odorant responses in WT and KO mice
A, normalized EOG responses to 100 ms pulses of vapour of the indicated amyl acetate concentration in solution for WT (black traces) or KO (grey traces). *B–D*, average values for latency (*B*), rise time (*C*), and time constant of the termination phase (*D*) were not significantly different in WT and KO animals at each odorant concentration ($n = 10$).

fitted with a single exponential function, while in Ringer solution containing 1 mM Ca^{2+}, the rising phase was slower and could not be described by a single exponential function. To better illustrate the rising phase, traces were normalized to their peak values and plotted superimposed on an expanded time scale in the insets of Fig. 4*A* and *B*. We measured the time necessary for the current to reach 50% of its maximal response, t_{50}, after the delivery of the light flash and found that the average ratio between t_{50} measured in Ringer solution and in low Ca^{2+} at -50 mV was 7.1 ± 3.0 ($n = 4$) for WT, not significantly different from the value of 9.1 ± 3.2 ($n = 5$) for KO.

To further investigate the presence of a Ca^{2+}-activated Cl^- current, we compared currents in Ringer solution containing 1 mM Ca^{2+} at $+50$ or -50 mV in the same

neuron (Fig. 4*C* and *D*). At $+50$ mV the influx of Ca^{2+} through CNG channels is greatly reduced and the outward current is mainly carried by K^+ ions, whose permeation through CNG channels is similar to that of Na^+ ions (reviewed in Kaupp & Seifert, 2002). Both in WT and KO, the rising phase at $+50$ mV could be well described by a single exponential function, whereas more than one current component was present at -50 mV, as discussed above. The different rising components are illustrated in more detail in the insets of Fig. 4*C* and *D*. The rising time of the response was measured, as described above, as t_{50}, and we found that the ratio between t_{50} at $+50$ and at -50 mV was 0.27 ± 0.13 ($n = 3$) for WT, not significantly different from the value of 0.22 ± 0.07 ($n = 4$) for KO. Furthermore, in the same set of experiments, the ratio
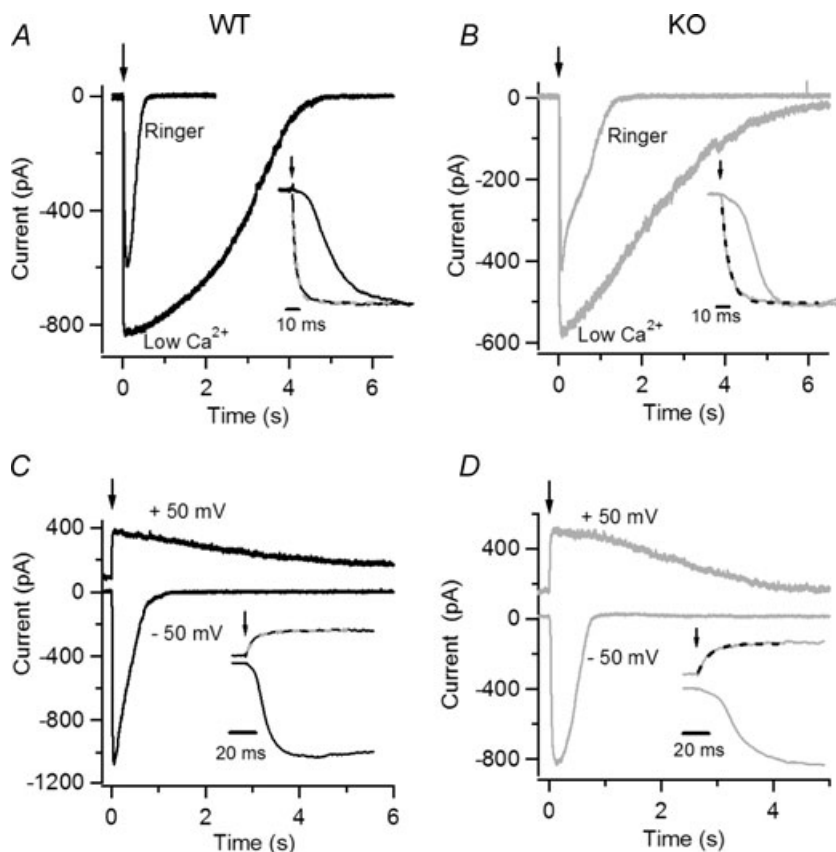
Figure 4. Current responses induced by photorelease of 8-Br-cAMP in isolated olfactory sensory neurons from WT and KO mice
Currents recorded from isolated mouse olfactory sensory neurons in the whole-cell voltage-clamp configuration in response to photorelease of 8-Br-cAMP in the cilia. An ultraviolet flash was applied at the time indicated by each arrow. *A* and *B*, an isolated olfactory sensory neuron from WT (*A*, black traces) and KO (*B*, grey traces) mice was bathed in Ringer solution containing 1 mM Ca^{2+} or in nominally 0 Ca^{2+} at the holding potential of -50 mV. Insets: responses were scaled to their maximum value and plotted superimposed on an expanded time scale. The rising phase of the response in 0 Ca^{2+} solution was fast and was well fitted by a single exponential (dashed lines), with $\tau = 3.6$ ms for WT and $\tau = 6.2$ ms for KO. Traces in Ringer solution and 0 Ca^{2+} in each panel were recorded from the same neuron. *C* and *D*, currents in an isolated olfactory sensory neuron from WT (*C*, black traces) and KO (*D*, grey traces) mice at the holding potential of -50 or $+50$ mV. Insets: current responses plotted on an expanded time scale, displayed a multiphasic rising phase at -50 mV, whereas at $+50$ mV the rising phase was well fitted by a single exponential (dashed lines, $\tau = 7.7$ ms for WT and $\tau = 10.9$ ms for KO mice). Traces at -50 and $+50$ mV in each panel were recorded from the same neuron.

between peak current amplitude at +50 and −50 mV was 0.35 ± 0.08 ($n = 3$) for WT, not significantly different from 0.43 ± 0.30 ($n = 4$) for KO mice.

These results show that in isolated olfactory sensory neurons from both mouse lines the transduction current comprises a primary CNG current and a secondary Ca²⁺-activated current that is expected to be carried by Cl⁻ ions (Boccaccio & Menini, 2007).

To directly measure Ca²⁺-activated currents in WT and KO mice, we photoreleased Ca²⁺ in the cilia (Fig. 5). To determine if Ca²⁺-activated currents were carried by Cl⁻, we measured the reversal potentials in the presence of various Cl⁻ concentrations. In a first set of experiments, we measured the reversal potential in almost symmetrical Cl⁻ solutions (Fig. 5A and B), while in a second set of experiments we reduced the intracellular Cl⁻ concentration by replacing most Cl⁻ with gluconate (Fig. 5C and D). The average reversal potential in symmetrical Cl⁻ solutions for WT, -0.8 ± 1.6 mV ($n = 5$), was not significantly different from that measured

in KO, -0.5 ± 3.2 mV ($n = 4$) (Fig. 5E). The average reversal potential in the low intracellular Cl⁻ solution was shifted toward more negative values, as expected for Cl⁻ channels in our ionic conditions, and was similar for WT, -37.0 ± 1.2 mV ($n = 5$), and KO, -41.7 ± 5.6 mV ($n = 5$) (Fig. 5E). These results confirm that Ca²⁺-activated Cl⁻ channels were present in olfactory sensory neurons from both WT and KO mice.

Currents in inside-out excised membrane patches from dendritic knob/cilia

To obtain a precise control of the concentrations of cyclic nucleotides and Ca²⁺ at the intracellular side of the transduction channels, we conducted patch-clamp experiments on excised membrane patches from the dendritic knob of dissociated olfactory sensory neurons with visible cilia of WT and KO mice. As previously noted (Reisert *et al.* 2003), cilia were sometimes sucked into the tip of the patch pipette and therefore the excised patches
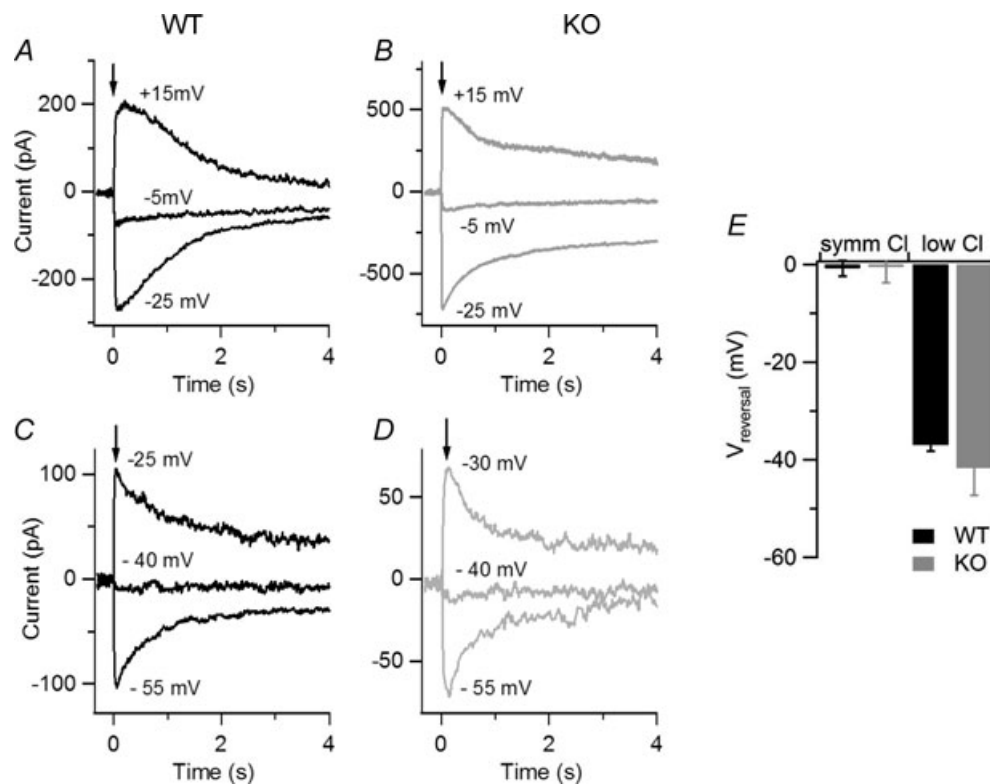

Figure 5. Current responses induced by photorelease of Ca²⁺ in isolated olfactory sensory neurons from WT and KO mice
Currents recorded from isolated mouse olfactory sensory neurons in the whole-cell voltage-clamp configuration in response to photorelease of caged Ca²⁺ (DMNP-EDTA) in the cilia. An ultraviolet flash was applied at the time indicated by each arrow to release the physiologically active Ca²⁺ into the ciliary region. *A* and *B*, currents from olfactory sensory neurons were recorded in symmetrical Cl⁻ solutions from WT (*A*, black traces) and KO (*B*, grey traces) mice. Currents in each panel were evoked on the same isolated olfactory sensory neuron at the indicated holding potentials, corrected for junction potentials. *C* and *D*, similar experiments were repeated when most (see Methods section) Cl⁻ in the intracellular solution was replaced with gluconate. *E*, average reversal potentials in symmetrical Cl⁻ solutions and in low Cl⁻ solutions.

contained membranes from both the dendritic knob and from the cilia.

To investigate the presence of CNG and Ca^{2+}-activated Cl^- currents, inside-out excised membrane patches, at the holding potential of -50 mV, were first exposed to a solution containing 100 μM cAMP in the absence of divalent cations. The same patch was then exposed to a solution containing 100 μM Ca^{2+} (Fig. 6A and B).
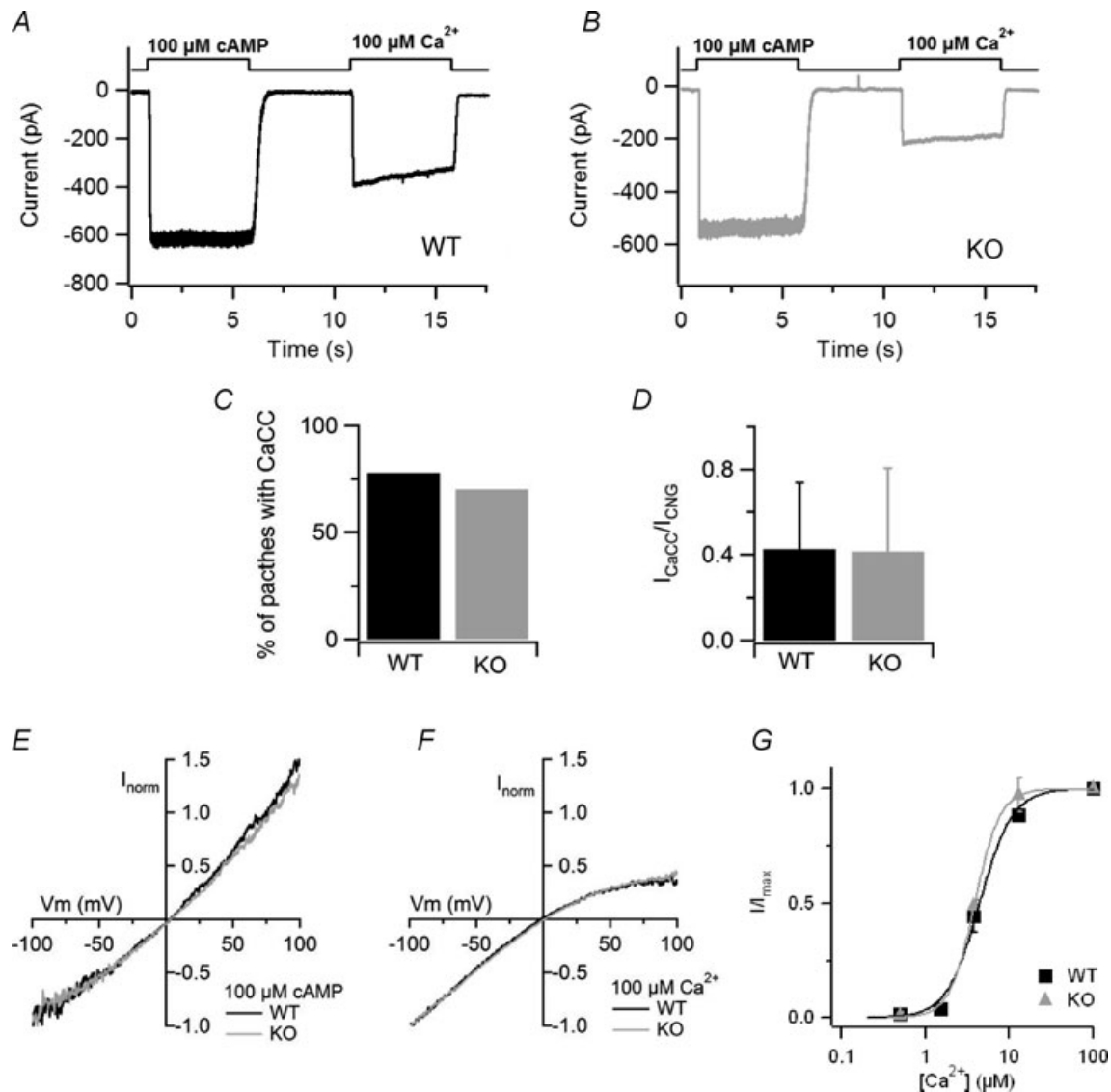
Figure 6. Recordings of CNG and Ca^{2+}-activated Cl^- currents in inside-out membrane patches
A and *B*, the cytoplasmic side of membrane patches excised from dendritic knob/cilia of olfactory sensory neurons from WT mice (*A*) and KO mice (*B*) was exposed to 100 μM cAMP, in the absence of divalent cations, to activate the CNG channels, and to 100 μM Ca^{2+} to activate the Cl^- channels. Divalent cations were absent from the patch pipette solution. The holding potential was -50 mV. *C*, percentage of membrane patches with detectable Ca^{2+}-activated Cl^- currents with respect to the presence of CNG currents in WT and KO mice. *D*, average ratios between Ca^{2+}-activated Cl^- currents and CNG currents in patches from WT (*n* = 6) and KO (*n* = 11) mice. *E*, comparison of representative current–voltage relations of the CNG current activated by 100 μM cAMP in WT (black trace) or KO (grey trace) patches. Voltage ramp from -100 to $+100$ mV. Currents were normalized to the value at -100 mV. *F*, comparison of representative current–voltage relations of the Cl^- current activated by 100 μM Ca^{2+} in WT (black trace) or KO (grey trace) patches. Voltage ramps from -100 to $+100$ mV. Currents were normalized to the value at -100 mV. *G*, dose–response relations were measured exposing patches to various free Ca^{2+} concentrations. The holding potential was -50 mV. Peak currents at each Ca^{2+} concentrations were normalized to the average current measured in the presence of 100 μM Ca^{2+} before and after each test Ca^{2+} concentration. Normalized currents were plotted *versus* Ca^{2+} concentrations, and fitted to the Hill equation. For WT mice $K_{1/2}$ was 4.4 μM, and n_H was 2.2 (*n* = 3). For KO mice $K_{1/2}$ was 3.8 μM, and n_H was 2.9 (*n* = 3).

We found that, both in WT and KO mice, about 75% of the membrane patches that showed detectable CNG currents also had Ca^{2+}-activated Cl$^-$ currents (Fig. 6C). We observed a great variability in current amplitudes in both mouse lines: at -50 mV, currents in WT mice varied from absolute values of 29 to 795 pA for CNG currents, and from 16 to 495 pA for Ca^{2+}-activated Cl$^-$ currents, while currents in KO mice varied from absolute values of 56 to 902 pA for CNG currents, and from 9 to 212 pA for Ca^{2+}-activated Cl$^-$ currents. Since it has been previously shown that Ca^{2+}-activated Cl$^-$ currents in olfactory sensory neurons exhibit a rundown over time, while CNG currents remain quite constant (Reisert et al. 2003), both currents were measured within 30 s after patch excision. The average CNG current at -50 mV was 327 ± 305 pA ($n = 7$) in WT animals, not significantly different from the value of 209 ± 254 pA ($n = 14$) in KO mice. For Ca^{2+}-activated Cl$^-$ currents the average amplitude at -50 mV was 113 ± 15 pA ($n = 7$) in WT animals, also not significantly different from the value of 44 ± 64 pA ($n = 14$) in KO mice. To obtain an estimate of the relative density of channels we measured the ratio between Ca^{2+}-activated Cl$^-$ currents and CNG currents in each membrane patch. The average ratio between Ca^{2+}-activated Cl$^-$ currents and CNG currents was 0.42 ± 0.31 ($n = 7$) in WT animals, not significantly different from the value of 0.41 ± 0.39 ($n = 14$) calculated in KO mice (Fig. 6D). These results show that Ca^{2+}-activated Cl$^-$ currents are present in inside-out patches from the dendritic knob/cilia of KO mice.

To further compare other biophysical properties of the transduction channels in WT and KO mice, we measured the rectification properties of the two types of currents. Currents were activated by 100 μM cAMP (Fig. 6E) or by 100 μM Ca^{2+} (Fig. 6F) using voltage ramps from -100 to $+100$ mV and normalized to the value at -100 mV. As shown in Fig. 6E and F, normalized current–voltage relations from WT and KO mice superimposed. The average ratio between currents at $+50$ and -50 mV for CNG currents was 1.13 ± 0.15 ($n = 5$) in WT animals, not significantly different from the value of 1.15 ± 0.15 ($n = 10$) calculated in KO mice. For Ca^{2+}-activated Cl$^-$ currents the average ratio between currents at $+50$ and -50 mV was 0.52 ± 0.20 ($n = 5$) in WT animals, also not significantly different from the value of 0.52 ± 0.08 ($n = 6$) in KO mice.

Since it has been previously shown (Reisert et al. 2003) that, in addition to rundown, Ca^{2+}-activated Cl$^-$ currents in olfactory sensory neurons also exhibit a reversible time-dependent decrease in amplitude during the exposure to a constant Ca^{2+} concentration (Fig. 6A and B), we measured the ratio between current amplitudes measured at the peak and after 5 s of 100 μM Ca^{2+} exposure. We found that the ratio was 0.80 ± 0.10 ($n = 6$)

in WT mice, not significantly different from the value of 0.78 ± 0.13 in KO animals ($n = 12$).

Finally, to measure the Ca^{2+} sensitivity of the Cl$^-$ channel in WT and KO mice, we obtained dose–response relations by activating currents with various Ca^{2+} concentrations in excised membrane patches (Fig. 6G). Experiments were performed after the rapid phase of rundown, when currents reached an almost steady-state value and, to take into account a remaining slow phase of the rundown that was present in some membrane patches, currents at each test Ca^{2+} concentration were normalized to the average current activated by 100 μM Ca^{2+} before and after each test Ca^{2+} concentration. Normalized currents measured at -50 mV were plotted versus Ca^{2+} concentration and fitted by the Hill equation: $I/I_{max} = c^{n_H}/(c^{n_H} + K_{1/2}^{n_H})$, where c is the Ca^{2+} concentration, $K_{1/2}$ the Ca^{2+} concentration producing half-maximal current activation, and n_H is the Hill coefficient. At -50 mV, the $K_{1/2}$ was 4.4 μM for WT, similar to 3.8 μM for KO mice, and n_H was 2.2 and 2.9 for WT and KO animals, respectively (Fig. 6G). $K_{1/2}$ and n_H values were not significantly different between WT and KO mice.

Thus, electrophysiological properties of Ca^{2+}-activated Cl$^-$ currents in inside-out membrane patches from dendritic knob/cilia of olfactory sensory neurons are not significantly different between WT and KO mice.

Discussion

Expression of Best2 in the ciliary layer of the olfactory epithelium

In this study, we confirmed that Best2 is expressed in the ciliary layer of olfactory sensory neurons and that the antibody against Best2 we previously developed (Pifferi et al. 2006b) is specific for this protein, as demonstrated by the absence of immunostaining in the olfactory epithelium of KO mice. Thus, these data, together with those of a very recently published study (Klimmeck et al. 2009) in which the expression of Best2 in the olfactory epithelium was extensively investigated, solve the reported controversy (Hartzell et al. 2008; Marmorstein et al. 2009) as to whether mouseBest2 is indeed expressed in the olfactory epithelium. In fact, Bakall et al. (2008), by employing immunoistochemistry in the same mouse lines of the present study, found expression of the Best2 protein in the colon and in the eye (in the non-pigmented epithelia cells of the ciliary body) of WT mice, but not in the olfactory epithelium, although they detected a Best2 transcript. A possible explanation of the different results between the laboratories is likely to reside in the different antibodies that were used. Indeed, Bakall et al. (2008) reported that their antibody was not working in Western blot. On the other side, concerning the immunohistochemistry, it must be noted that no positive controls of the immunostaining

in the olfactory epithelium were shown by Bakall *et al.* (2008) and therefore it cannot be excluded that, since cilia are very fragile, they were absent from the olfactory epithelium slices.

Physiological role of Best2

Since Best2 is expressed in the cilia of olfactory sensory neurons (Pifferi *et al.* 2006*b*), the site of olfactory transduction, and it has been previously demonstrated that Best2 forms Ca^{2+}-activated Cl^- channels when expressed in heterologous systems (Qu *et al.* 2004; Qu & Hartzell, 2004; Pifferi *et al.* 2006*b*), we conducted experiments to investigate the physiological role of Best2 in olfactory transduction by comparing the properties of WT mice with those of KO mice. Since a previous study has shown that KO mice showed no obvious olfactory deficits, as detected by the cookie test (Bakall *et al.* 2008), we also repeated this type of behavioural test and found results in agreement with those previously published. However, it cannot be concluded from these experiments that Best2 is not required for normal olfactory sensitivity, as more detailed behavioural studies, as for example the study of olfactory behavioural thresholds as reported in mice lacking NKCC1 (Smith *et al.* 2008), would be required to reach such a conclusion. In addition, it is important to note that, as previously pointed out by Smith *et al.* (2008), it is still unknown whether a deficit in Ca^{2+}-activated Cl^- current would produce a reduction in olfactory sensitivity, and it is possible that the secondary Cl^- current may not be required at all for normal olfactory sensitivity. Indeed, it is possible that the primary current through CNG channels is sufficient for normal olfactory sensitivity.

We analysed the responses to odorants of the olfactory epithelium and found no differences in the odorant sensitivity or kinetics properties measured by EOG recordings in WT and KO mice. Moreover, at the level of single olfactory sensory neurons, a Ca^{2+}-activated Cl^- channel component was also measured by using photolysis of caged 8-Br-cAMP or of caged Ca^{2+} localized to the cilia of olfactory sensory neurons of KO mice. Finally, a Ca^{2+}-activated Cl^- current was still present in excised inside-out patches from knob/cilia of olfactory sensory neurons of KO mice, with electrophysiological properties similar to those of WT mice.

Thus, we determined that the absence of expression of Best2 in the ciliary layer of the olfactory epithelium does not significantly alter the electrophysiological properties of the olfactory epithelium. These results indicate that Best2 may not be the main molecular component of the olfactory Ca^{2+}-activated Cl^- channel, although we cannot exclude the possibility that in KO mice some compensatory mechanisms may act to replace the function of the missing protein. However, it must also

be noted here that, although the protein Best2 has been proposed as a candidate for being a molecular component of the olfactory Ca^{2+}-activated Cl^- channel, very recent studies reported that the anoctamin/TMEM16 family of membrane proteins display many features of native Ca^{2+}-activated Cl^- channels (Caputo *et al.* 2008; Schroeder *et al.* 2008; Yang *et al.* 2008). In addition, it has been shown, by *in situ* hybridization, that TMEM16B is expressed in the mature sensory neurons of the mouse olfactory epithelium (Yu *et al.* 2005), and it is a prominent protein in the rat olfactory ciliary proteome (transmembrane protein 16B isoform 2, Supplementary Table S1 in Mayer *et al.* 2009). Stephan *et al.* (2009) also identified TMEM16B (Anoctamin 2, ANO2) in a proteomic screen of ciliary membranes and showed that the fusion protein TMEM16B-EGFP localized to the cilia when expressed *in vivo* using an adenoviral vector. In addition, Stephan *et al.* (2009) provided evidence that the electrophysiological properties of this protein are remarkably similar to those of native olfactory Ca^{2+}-activated Cl^- channels.

We have also recently characterized the electrophysiological properties of the mouse TMEM16B expressed in a heterologous system and found that the channel properties are remarkably similar to those of the native Ca^{2+}-activated Cl^- channels (Pifferi *et al.* 2009). Indeed, while we have previously pointed out that a significant difference between Best2 and the native olfactory channel was a Ca^{2+} sensitivity difference of one order of magnitude, with a Ca^{2+} concentration for half-maximal activation at -50 mV of 0.4 μM for Best2 and a higher concentration of 4.7 μM for native channels (Pifferi *et al.* 2006*b*), we recently showed that the $K_{1/2}$ for Ca^{2+} in TMEM16B-induced currents was 4.9 μM, similar to the native channel. Further studies will have to establish whether TMEM16B is a component of the olfactory Ca^{2+}-activated Cl^- channel.

In this study, we have shown that Best2 is expressed in the olfactory ciliary layer, but it does not appear to be the main molecular component of the Ca^{2+}-activated Cl^- current. What is then the physiological role of Best2 in the olfactory epithelium? In addition to functioning as Ca^{2+}-activated Cl^- channels when expressed heterologously, mouse Best2 and other bestrophins have also been shown to be activated by osmotic cell swelling in the absence of Ca^{2+}, indicating that they may be cell volume regulators (Fischmeister & Hartzell, 2005; Chien & Hartzell, 2007). Furthermore, Best1 can interact with the voltage-gated Ca^{2+} channel Cav1.3 and modulate its biophysical properties (Rosenthal *et al.* 2006; Yu *et al.* 2008), indicating that some bestrophins could also act as regulators of other ion channels. In the eye, Best2 is expressed in the non-pigmented epithelium and, using the same mouse line employed in the present study, it was found that KO mice have a diminished

intraocular pressure compared to WT mice (Bakall *et al.* 2008). A very recent study suggested that Best2 is involved in the control of aqueous dynamics (Zhang *et al.* 2009).

In the olfactory epithelium, Klimmeck *et al.* (2009) have recently investigated in detail the expression pattern of Best2 comparing results from adult and postnatal day 1 (P1) mice. In adult mice, whose olfactory epithelium contains mainly mature olfactory sensory neurons, Best2 expression was found in the cilia of these neurons. In P1 mice, where most olfactory sensory neurons are still immature, strong Best2 signals were detected at all subcellular levels of the developing neurons. Based on these observations, Klimmeck *et al.* (2009) suggested a physiological role for Best2 related to neurogenesis, in which Best2 may act as a volume-regulated anion channel contributing to the coordinated extension of cell volume in developing sensory neurons.

In the olfactory cilia, it is possible to speculate that Best2 may subserve different functions as, for example, the maintenance of the local ionic homeostasis, also preventing volume changes resulting from the exposure to exogenous osmotically active solutions. It is also possible to envisage that Best2 could contribute to setting the correct chloride concentration in the mucous layer of the olfactory epithelium.

In summary, we now have unequivocal confirmation that Best2 is expressed in the cilia of mature olfactory sensory neurons, thus cutting out all the controversies about its presence in the olfactory epithelium. Nevertheless, the function of Best2 remains elusive and further studies will be required to determine its physiological role.

References

Bakall B, McLaughlin P, Stanton JB, Zhang Y, Hartzell HC, Marmorstein LY & Marmorstein AD (2008). Bestrophin-2 is involved in the generation of intraocular pressure. *Invest Ophthalmol Vis Sci* **49**, 1563–1570.

Boccaccio A, Lagostena L, Hagen V & Menini A (2006). Fast adaptation in mouse olfactory sensory neurons does not require the activity of phosphodiesterase. *J Gen Physiol* **128**, 171–184.

Boccaccio A & Menini A (2007). Temporal development of cyclic nucleotide-gated and Ca^{2+}-activated Cl^{--} currents in isolated mouse olfactory sensory neurons. *J Neurophysiol* **98**, 153–160.

Caputo A, Caci E, Ferrera L, Pedemonte N, Barsanti C, Sondo E, Pfeffer U, Ravazzolo R, Zegarra-Moran O & Galietta LJ (2008). TMEM16A, a membrane protein associated with calcium-dependent chloride channel activity. *Science* **322**, 590–594.

Chien LT & Hartzell HC (2007). *Drosophila* bestrophin-1 chloride current is dually regulated by calcium and cell volume. *J Gen Physiol* **130**, 513–524.

Firestein S (2001). How the olfactory system makes sense of scents. *Nature* **413**, 211–218.

Fischmeister R & Hartzell HC (2005). Volume sensitivity of the bestrophin family of chloride channels. *J Physiol* **562**, 477–491.

Franceschini V, Bettini S, Pifferi S, Rosellini A, Menini A, Saccardi R, Ognio E, Jeffery R, Poulsom R & Revoltella RP (2009). Human cord blood CD133+ stem cells transplanted to nod-scid mice provide conditions for regeneration of olfactory neuroepithelium after permanent damage induced by dichlobenil. *Stem Cells* **27**, 825–835.

Frings, S (2009). Chloride-based signal amplification in olfactory sensory neurons. In *Physiology and Pathology of Chloride Transporters and Channels in the Nervous System. From Molecules to Diseases*, ed. Alvarez-Leefmans FJ & Delpire E. Elsevier–Academic Press, San Diego.

Frings S, Reuter D & Kleene SJ (2000). Neuronal Ca^{2+}-activated Cl^{--} channels: homing in on an elusive channel species. *Prog Neurobiol* **60**, 247–289.

Hartzell C, Putzier I & Arreola J (2005). Calcium-activated chloride channels. *Annu Rev Physiol* **67**, 719–758.

Hartzell HC, Qu Z, Yu K, Xiao Q & Chien LT (2008). Molecular physiology of bestrophins: multifunctional membrane proteins linked to best disease and other retinopathies. *Physiol Rev* **88**, 639–672.

Hartzell HC, Yu K, Xiao Q, Chien LT & Qu Z (2009). Anoctamin/TMEM16 family members are Ca^{2+}-activated Cl$^-$ channels. *J Physiol* **587**, 2127–2139.

Kaneko H, Nakamura T & Lindemann B (2001). Noninvasive measurement of chloride concentration in rat olfactory receptor cells with use of a fluorescent dye. *Am J Physiol Cell Physiol* **280**, C1387–C1393.

Kaneko H, Putzier I, Frings S, Kaupp UB & Gensch T (2004). Chloride accumulation in mammalian olfactory sensory neurons. *J Neurosci* **24**, 7931–7938.

Kaupp UB & Seifert R (2002). Cyclic nucleotide-gated ion channels. *Physiol Rev* **82**, 769–824.

Kleene SJ (1993). Origin of the chloride current in olfactory transduction. *Neuron* **11**, 123–132.

Kleene SJ (1997). High-gain, low-noise amplification in olfactory transduction. *Biophys J* **73**, 1110–1117.

Kleene SJ (2008). The electrochemical basis of odor transduction in vertebrate olfactory cilia. *Chem Senses* **33**, 839–859.

Kleene SJ & Gesteland RC (1991). Calcium-activated chloride conductance in frog olfactory cilia. *J Neurosci* **11**, 3624–3629.

Klimmeck D, Daiber PC, Brühl A, Baumann A, Frings S & Möhrlen F (2009). Bestrophin 2: an anion channel associated with neurogenesis in chemosensory systems. *J Comp Neurol* **515**, 585–599.

Kunzelmann K, Milenkovic VM, Spitzner M, Soria RB & Schreiber R (2007). Calcium-dependent chloride conductance in epithelia: is there a contribution by bestrophin? *Pflugers Arch* **454**, 879–889.

Kurahashi T & Yau KW (1993). Co-existence of cationic and chloride components in odorant-induced current of vertebrate olfactory receptor cells. *Nature* **363**, 71–74.

Lagostena L & Menini A (2003). Whole-cell recordings and photolysis of caged compounds in olfactory sensory neurons isolated from the mouse. *Chem Senses* **28**, 705–716.

Lowe G & Gold GH (1993). Nonlinear amplification by calcium-dependent chloride channels in olfactory receptor cells. *Nature* **366**, 283–286.

Malnic B (2007). Searching for the ligands of odorant receptors. *Mol Neurobiol* **35**, 175–181.

Marmorstein AD, Cross HE & Peachey NS (2009). Functional roles of bestrophins in ocular epithelia. *Prog Retin Eye Res* **28**, 206–226.

Matthews HR & Reisert J (2003). Calcium, the two-faced messenger of olfactory transduction and adaptation. *Curr Opin Neurobiol* **13**, 469–475.

Mayer U, Kuller A, Daiber PC, Neudorf I, Warnken U, Schnolzer M, Frings S & Mohrlen F (2009). The proteome of rat olfactory sensory cilia. *Proteomics* **9**, 322–334.

Menini A (1999). Calcium signalling and regulation in olfactory neurons. *Curr Opin Neurobiol* **9**, 419–426.

Menini A, Lagostena L & Boccaccio A (2004). Olfaction: from odorant molecules to the olfactory cortex. *News Physiol Sci* **19**, 101–104.

Meyer MR, Angele A, Kremmer E, Kaupp UB & Muller F (2000). A cGMP-signaling pathway in a subset of olfactory sensory neurons. *Proc Natl Acad Sci U S A* **97**, 10595–10600.

Ottoson D (1955). Analysis of the electrical activity of the olfactory epithelium. *Acta Physiol Scand Suppl* **35**, 1–83.

Patton C, Thompson S & Epel D (2004). Some precautions in using chelators to buffer metals in biological solutions. *Cell Calcium* **35**, 427–431.

Pifferi S, Boccaccio A & Menini A (2006*a*). Cyclic nucleotide-gated ion channels in sensory transduction. *FEBS Lett* **580**, 2853–2859.

Pifferi S, Dibattista M & Menini A (2009). TMEM16B induces chloride currents activated by calcium in mammalian cells. *Pflugers Arch* (in press; doi: 10.1007/s00424-009-0684-9).

Pifferi S, Pascarella G, Boccaccio A, Mazzatenta A, Gustincich S, Menini A & Zucchelli S (2006*b*). Bestrophin-2 is a candidate calcium-activated chloride channel involved in olfactory transduction. *Proc Natl Acad Sci U S A* **103**, 12929–12934.

Pusch M (2004). Ca^{2+}-activated chloride channels go molecular. *J Gen Physiol* **123**, 323–325.

Qu Z, Fischmeister R & Hartzell C (2004). Mouse bestrophin-2 is a bona fide Cl^- channel: identification of a residue important in anion binding and conduction. *J Gen Physiol* **123**, 327–340.

Qu Z & Hartzell C (2004). Determinants of anion permeation in the second transmembrane domain of the mouse bestrophin-2 chloride channel. *J Gen Physiol* **124**, 371–382.

Qu Z, Wei RW, Mann W & Hartzell HC (2003). Two bestrophins cloned from *Xenopus laevis* oocytes express Ca^{2+}-activated Cl^- currents. *J Biol Chem* **278**, 49563–49572.

Reisert J, Bauer PJ, Yau KW & Frings S (2003). The Ca-activated Cl channel and its control in rat olfactory receptor neurons. *J Gen Physiol* **122**, 349–363.

Reuter D, Zierold K, Schroder WH & Frings S (1998). A depolarizing chloride current contributes to chemoelectrical transduction in olfactory sensory neurons in situ. *J Neurosci* **18**, 6623–6630.

Rodriguez I (2007). Odorant and pheromone receptor gene regulation in vertebrates. *Curr Opin Genet Dev* **17**, 465–470.

Rosenthal R, Bakall B, Kinnick T, Peachey N, Wimmers S, Wadelius C, Marmorstein A & Strauss O (2006). Expression of bestrophin-1, the product of the VMD2 gene, modulates voltage-dependent Ca^{2+} channels in retinal pigment epithelial cells. *FASEB J* **20**, 178–180.

Schild D & Restrepo D (1998). Transduction mechanisms in vertebrate olfactory receptor cells. *Physiol Rev* **78**, 429–466.

Schroeder BC, Cheng T, Jan YN & Jan LY (2008). Expression cloning of TMEM16A as a calcium-activated chloride channel subunit. *Cell* **134**, 1019–1029.

Scott JW & Scott-Johnson PE (2002). The electroolfactogram: a review of its history and uses. *Microsc Res Tech* **58**, 152–160.

Smith DW, Thach S, Marshall EL, Mendoza MG & Kleene SJ (2008). Mice lacking NKCC1 have normal olfactory sensitivity. *Physiol Behav* **93**, 44–49.

Stephan AB, Shum EY, Hirsh S, Cygnar KD, Reisert J & Zhao H (2009). ANO2 is the cilial calcium-activated chloride channel that may mediate olfactory amplification. *Proc Natl Acad Sci U S A* (in press; doi: 10.1073/pnas. 0903304106).

Sun H, Tsunenari T, Yau KW & Nathans J (2002). The vitelliform macular dystrophy protein defines a new family of chloride channels. *Proc Natl Acad Sci U S A* **99**, 4008–4013.

Tsunenari T, Sun H, Williams J, Cahill H, Smallwood P, Yau KW & Nathans J (2003). Structure-function analysis of the bestrophin family of anion channels. *J Biol Chem* **278**, 41114–41125.

Yang YD, Cho H, Koo JY, Tak MH, Cho Y, Shim WS, Park SP, Lee J, Lee B, Kim BM, Raouf R, Shin YK & Oh U (2008). TMEM16A confers receptor-activated calcium-dependent chloride conductance. *Nature* **455**, 1210–1215.

Yu K, Xiao Q, Cui G, Lee A & Hartzell HC (2008). The best disease-linked Cl^- channel hBest1 regulates Ca_V1 (L-type) Ca^{2+} channels via src-homology-binding domains. *J Neurosci* **28**, 5660–5670.

Yu TT, McIntyre JC, Bose SC, Hardin D, Owen MC & McClintock TS (2005). Differentially expressed transcripts from phenotypically identified olfactory sensory neurons. *J Comp Neurol* **483**, 251–262.

Zhang Y, Davidson BR, Stamer WD, Barton JK, Marmorstein LY & Marmorstein AD (2009). Enhanced inflow and outflow rates despite lower IOP in bestrophin-2-deficient mice. *Invest Ophthalmol Vis Sci* **50**, 765–770.

Author contributions

Authors' present addresses

S. Pifferi: Max Delbrück Center for Molecular Medicine (MDC), Berlin-Buch, Germany.
A. Boccaccio: Italian Institute of Technology, Department of Neuroscience and Brain Technologies, Genova, Italy.